

# Hadron Physics and Lattice QCD

Constantia Alexandrou

*Department of Physics, University of Cyprus, P.O. Box 20537, 1678 Nicosia, Cyprus and  
Computational-based Science and Technology Research Center, The Cyprus Institute, P.O. Box  
27456, CY-1645 Nicosia, Cyprus*

**Abstract.** A review of recent lattice QCD hadron structure calculations is presented. Important hadronic properties such as the axial charge and spin content of the nucleon, as well as, the mass and axial charge of hyperons and charmed baryons are discussed.

**Keywords:** Hadron Structure, Lattice QCD

**PACS:** 11.15.Ha, 12.38.Gc, 12.38.Aw, 12.38.-t, 14.70.Dj

## INTRODUCTION

The recent progress in the numerical simulation of the fundamental theory of the strong interactions, Quantum Chromodynamics (QCD), has been remarkable. Improvement in algorithms coupled with increase in computational power have enabled simulations to be carried out at near physical parameters of the theory. This opens up exciting possibilities for *ab Initio* reliable calculation of experimentally measured quantities as well as for predicting quantities that are not easily accessible to experiment. During the last decade, results from simulations of QCD have emerged that already provide essential input for a wide range of strong interaction phenomena as, for example, the QCD phase diagram, the structure of hadrons, nuclear forces and weak decays. In this presentation we focus on hadron structure calculations using state-of-the art lattice QCD simulations [1, 2, 3]. Understanding nucleon structure from first principles is considered a milestone of hadronic physics and a rich experimental program has been devoted to its study, starting with the measurements of the electromagnetic nucleon form factors initiated more than 50 years ago. Reproducing these key observables within the lattice QCD formulation is a prerequisite to obtaining reliable predictions on observables that explore Physics beyond the standard model.

The starting point of lattice QCD (LQCD) is a definition of the theory on a four-dimensional Euclidean space-time lattice with gauge fields defined as links between adjacent lattice sites and quarks defined at each lattice site as anticommuting Grassmann variables belonging to the fundamental representation of SU(3) [4]. It can be simulated on the computer using methods analogous to those used in Statistical Mechanics allowing calculation of matrix elements of any operator between hadronic states in terms of the fundamental quark and gluon degrees of freedom. The discretization the QCD Lagrangian is not unique and this is reflected in the variety of lattice actions of QCD that are in use today. It is customary to classify them according to the discretization of the fermionic part of the Lagrangian, the most common being improved Wilson-type such as Clover and twisted mass (TM) fermions, staggered fermions, domain wall (DW) and

overlap fermions. The latter two preserve chiral symmetry but are more expensive to simulate. Although LQCD provides an *ab Initio* calculation of hadronic properties, the discretization of space-time and the numerical simulation on a finite volume introduce artifacts that may lead to systematic errors, which must be carefully investigated before comparing to experimental results. Since simulations become increasingly harder as the quark mass is decreased to its physical value, LQCD simulations were up to very recently being carried out for quark masses larger than physical. Currently, simulations close or even at the physical value of the pion mass are being produced and analyzed.

## RECENT RESULTS

### Hadron masses

Masses of low-lying hadrons are considered benchmark quantities for LQCD. They are computed by evaluating the vacuum expectation value of two-point functions. Recent results using Clover [5] and TM fermion actions [6] with a careful analysis of lattice systematics have been obtained showing agreement with the experimental values. The QCDSF-UKQCD [7] and PACS-CS collaborations [8] have also performed spectrum studies using Clover fermions. Recent results using staggered [9], domain wall fermions (DWF) [10], and a mixed action approach with staggered sea quarks and DW valence quarks [11] show overall consistency [12]. This is a significant validation of LQCD.

There has been remarkable progress recently in computing masses of excited states of hadrons, notably by the Hadron Spectrum Collaboration using anisotropic lattices with a fine lattice spacing in the temporal direction that leads to an improved resolution of excited states [13]. Experimental searches of charmed hadrons have received significant attention, mainly due to the experimental observation of candidates of the doubly charmed baryons  $\Xi_{cc}^+(3520)$  and  $\Xi_{cc}^{++}(3460)$  by the SELEX collaboration [14, 15, 16]. No evidence was found for these states by the BABAR experiment [17] and FOCUS Collaboration [18]. The BELLE Collaboration [19] finds  $\Xi$ -states lower in mass, that can be candidates of excited states of  $\Xi_c$  but no doubly charmed cascade. Therefore, it is interesting to compute these masses in LQCD and compare with the experimental values. A mixed action approach is in general adopted with the charm valence quark being introduced on dynamical gauge configurations, which are produced with either staggered sea [20, 21, 22] or TM [23] fermions. A comparison of recent LQCD results on the masses of charmed baryons is provided in Fig. 1. There is an overall agreement among LQCD results apart from the mass of  $\Xi_{cc}$ . Although for  $\Xi_{cc}$  a value consistent with the result of the SELEX experiment is obtained with TM fermions (TMF), further study is required to understand the results among different lattice computations in order to reach a final conclusion. In Fig. 1 we also compare results for the spin 3/2 charmed baryons [23]. There is good agreement among lattice results and with the known experimental values for  $\Sigma_c^*$ ,  $\Xi_c^*$  and  $\Omega_c^*$ . Thus the lattice results can be taken as a prediction for the masses of the charmed spin-3/2 baryons  $\Xi_{cc}^*$ ,  $\Omega_{cc}^*$  and  $\Omega_{ccc}$ .

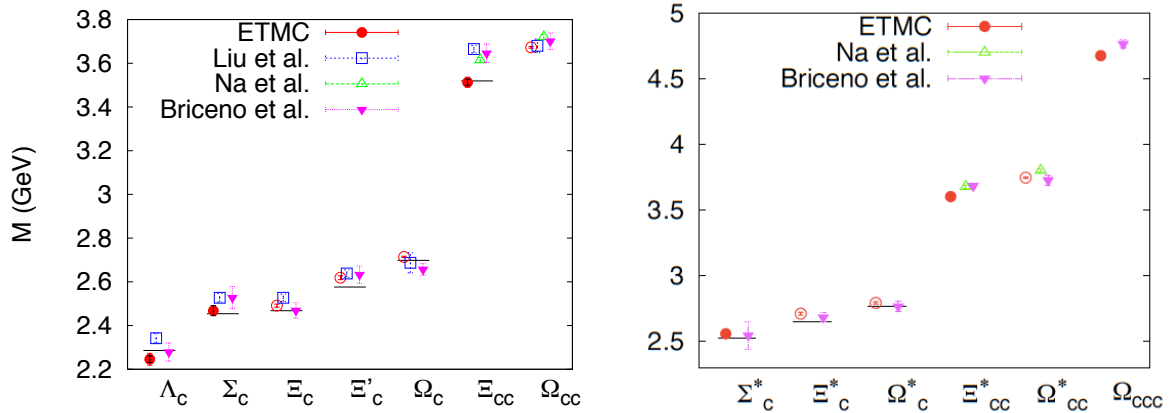
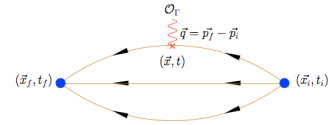


**FIGURE 1.** Masses of charmed baryons with spin 1/2 (left) and spin 3/2 (right) computed within lattice QCD. The experimental values are shown by the horizontal lines. With red filled circles, we show TMF results extrapolated to the physical pion mass whereas open circles shows the results obtained at  $m_\pi = 260$  MeV [23]. Results obtained using a number of hybrid actions with staggered sea quarks are from Refs. [21] (open blue squares), [20] (open green triangles) and [22] (filled magenta triangles).

## Hadron From factors

Calculation of hadron matrix elements of the form  $\langle h_f(\vec{p}_f) | \mathcal{O} | h_i(\vec{p}_i) \rangle$  requires both the evaluation of two- and three-point functions [2].

**Nucleon axial charge:** There is a number of LQCD calculations of the nucleon axial charge  $g_A$ , which is considered a benchmark quantity for form factor calculations within LQCD. The reason for this is that it is both well known experimentally and it can be determined at momentum transfer squared  $q^2 = (p_f - p_i)^2 = 0$  with no ambiguity associated with having to fit the  $q^2$ -dependence of the form factor (FF), as for example, in the case of the anomalous magnetic moment where one needs to fit the small  $q^2$ -dependence of the magnetic FF. In addition, only the connected diagram where the axial current couples to a valence quark as shown in the diagram, contributes. The computational cost is about twice that of a two-point function involved in the calculation of hadron masses.



In Fig. 2 we show recent LQCD results using TMF, Clover fermions, DWF and a hybrid action of DWF on a staggered sea, all of which are renormalized non-perturbatively. As can be seen, there is a nice agreement among different lattice discretizations and no significant dependence on the quark mass down to about  $m_\pi = 250$  MeV. Clover results with  $N_f = 2 + 1$  at  $m_\pi \sim 150$  MeV [24] and  $N_f = 2$  at  $m_\pi \sim 180$  MeV [25] underestimate the value of  $g_A$ . The origin of this discrepancy is being investigated.

A possible explanation for the observed discrepancy could come from excited states contamination. A dedicated high accuracy study of excited state contributions showed

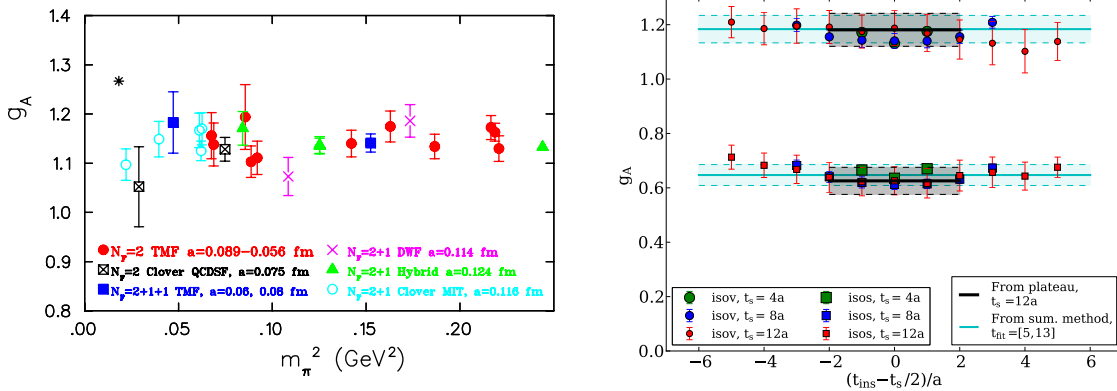


**FIGURE 2.** Left: Recent LQCD results on  $g_A$  using  $N_f = 2$  TMF [26] (filled circles),  $N_f = 2 + 1 + 1$  TMF (filled squares),  $N_f = 2 + 1$  DWF [27] (crosses),  $N_f = 2 + 1$  hybrid action [28] (filled triangles)  $N_f = 2$  Clover [25] (square with cross) and  $N_f = 2 + 1$  Clover [24] (open circles). The experimental value is shown by the asterisk. Right: Study of excited state contributions on  $g_A$  for various time source-sink separations  $t_s$ . The light blue band is the result of summation method. The upper plateau is for the isovector axial current whereas the lower for the isoscalar.

that for  $m_\pi \sim 400$  MeV there is no significant effect on the value extracted for  $g_A$  [29]. This is illustrate in Fig. 2 where the time separation between sink and source is varied from  $t_s = 4a$  to  $t_s = 12a$ . As can be seen, the same plateau value is obtained for all time separations. The same value is also obtained from another approach that involves summing the time where the axial current couples to the quark inside the nucleon. This demonstrates that excited state contamination is negligible at least for  $m_\pi \sim 400$  MeV. An assessment of volume and cut-off effects was also carried out [26] indicating that, for pion masses larger than  $m_\pi \sim 300$  MeV, volume and discretization errors are small compared to the uncertainty in the chiral extrapolation. This uncertainty is, however, eliminated by the recent result at almost physical pion mass, which, if confirmed by further studies, confronts us with a challenge.

**Axial charge for hyperons and charmed baryons:** The axial couplings of hyperons are either less well measured or not known experimentally. One relies on theoretical estimates, which can have large uncertainties. These couplings are phenomenologically important parameters within effective field theory descriptions. Using LQCD one can evaluate these axial couplings using the techniques employed in the case of the nucleon  $g_A$ , i.e. they are determined by the connected part of the appropriate hadron matrix element of the axial vector current at zero momentum transfer.

A first lattice QCD calculation of the axial charge of spin-1/2 hyperons was carried out using staggered sea quarks and DW valence quarks [30]. Using  $N_f = 2 + 1 + 1$  TMF the axial charges of hyperons and charmed baryons are calculated using the fixed current method that enables the computations of the axial charge of all hadrons with one sequential inversion, i.e. with the same number of inversions as for the case of the nucleon axial charge. The SU(3) symmetry relation  $g_A^N = F + D$ ,  $g_A^\Sigma = 2F$ ,  $g_A^\Xi = -D + F$  leading to  $g_A^N - g_A^\Sigma + g_A^\Xi = 0$  is shown as a function of the breaking parameter  $x = (m_K^2 - m_\pi^2)/(4\pi^2 f_\pi^2)$  in Fig. 3 for both TMF and hybrid results. The SU(3) symmetry breaking  $\delta_{\text{SU}(3)} = g_A^N - g_A^\Sigma + g_A^\Xi$  has an  $x^2$ -dependence yielding at the

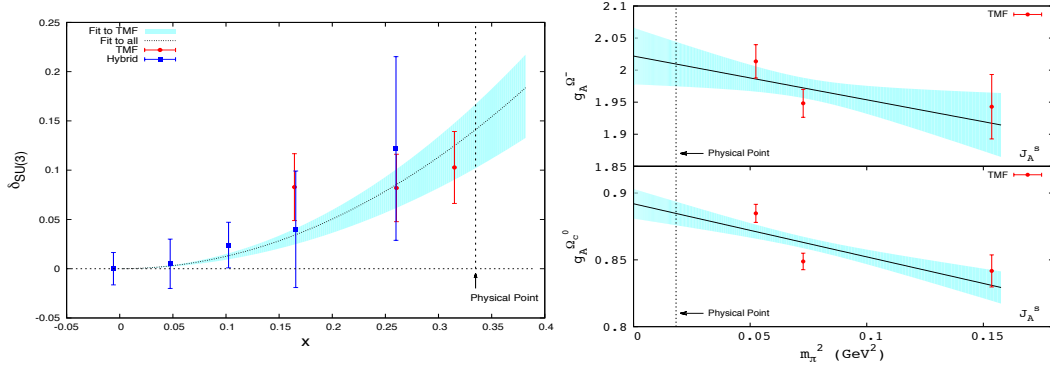


**FIGURE 3.** Left:  $\delta_{\text{SU}(3)} = g_A^N - g_A^\Sigma + g_A^\Xi$  versus  $x$  for TMF (red filled circles) and hybrid (blue filled squares) results [30]. The line is a fit to all data whereas the blue band to the TMF results. Right: The axial charge of  $\Omega^-$  and  $\Omega_c^0$  versus  $m_\pi^2$ .

physical point  $\delta_{\text{SU}(3)} \sim 15\%$ . First results for the decuplet axial charges  $g_A^\Delta$ ,  $g_A^{\Sigma^*}$  and  $g_A^{\Xi^*}$  indicate an even smaller SU(3) symmetry breaking. In Fig. 3 we show first results using  $N_f = 2 + 1 + 1$  TMF for the  $\Omega$  axial charge  $g_A^\Omega$  as a function of  $m_\pi^2$ .

**Nucleon Dirac and Pauli isovector radii and anomalous magnetic moment:** The nucleon Dirac and Pauli radii can be determined from  $r_{1,2}^2 = -\frac{6}{F_{1,2}(0)} \frac{dF_{1,2}}{dq^2} \Big|_{q^2=0}$  where the form factors  $F_1$  and  $F_2$  are extracted from nucleon matrix element of the electromagnetic current:  $\langle N(p_f) | j^\mu(0) | N(p_i) \rangle = \bar{u}_N(p_f) \left[ \gamma^\mu F_1(q^2) + \frac{i\sigma^{\mu\nu} q_\nu}{2m} F_2(q^2) \right] u_N(p_i)$ . It is customary to use a dipole Ansatz to fit the  $q^2$ -dependence of  $F_1$  and  $F_2$ . The anomalous magnetic moment is then given by  $F_2(0) \frac{m_N^{\text{phys}}}{m_N^{\text{lat}}}$  in Bohr magnetons. A number of LQCD collaborations have computed the *isovector* nucleon Dirac and Pauli form factors  $F_1$  and  $F_2$ , which in the isospin limit, gives the FFs of the proton minus that of the neutron. These isovector quantities only receive connected contributions and are thus computationally straight forward to calculate.

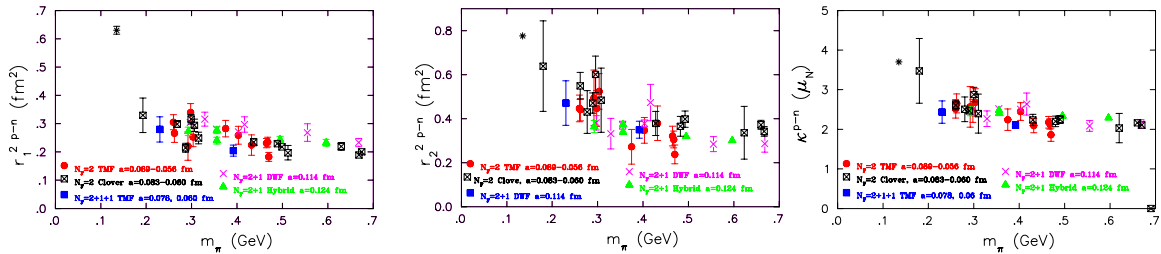


**FIGURE 4.** Dirac (left), Pauli (middle) rms radii and the nucleon anomalous magnetic moment (right) using  $N_f = 2$  [31] and  $N_f = 2 + 1 + 1$  [32] TMF,  $N_f = 2$  Clover fermions [33],  $N_f = 2 + 1$  DWF [34, 27] and a hybrid action of staggered sea and DW valence quarks [28].

In Fig. 4 we collect the most recent LQCD results on the isovector Dirac and Pauli radii, and anomalous magnetic moment. As can be seen, LQCD results are in agreement even before taking the continuum limit, which indicates that cut-off effects are small. Recent results at  $m_\pi \sim 180$  MeV [33] show an increase towards the physical value. The less rapid fall-off of baryon FFs with  $q^2$ , responsible for the smaller values of the radii,

is a common feature in current lattice QCD calculations that is under investigation.

## Nucleon spin

In order to extract information on the spin content of the nucleon one needs to evaluate the isoscalar moments  $A_{20}^{u+d}$  and  $B_{20}^{u+d}$  since the total spin of a quark in the nucleon is given by  $J^q = \frac{1}{2}(A_{20}^q + B_{20}^q)$ . The total spin can be further decomposed into its orbital angular momentum  $L^q$  and its spin component  $\Delta\Sigma^q$  as  $J^q = \frac{1}{2}\Delta\Sigma^q + L^q$ . The spin carried by the u- and d- quarks is determined using  $\Delta\Sigma^{u+d} = \tilde{A}_{10}^{u+d} = g_A^{IS}$ . In order to evaluate the isoscalar quantities one would need the disconnected contributions. These are notoriously difficult to calculate and they are neglected in most current evaluations. A recent calculation of the quark spin, which included the disconnected contributions was carried out using Clover fermions giving  $\Delta u + \Delta d + \Delta s = 0.45(4)(9)$  with  $\Delta s = -0.020(10)(4)$  at  $\mu = \sqrt{7.4}$  GeV [35]. This calculation shows that the strange quark contribution to the nucleon spin is small, a result consistent with COMPASS [36] and HERMES data [37].

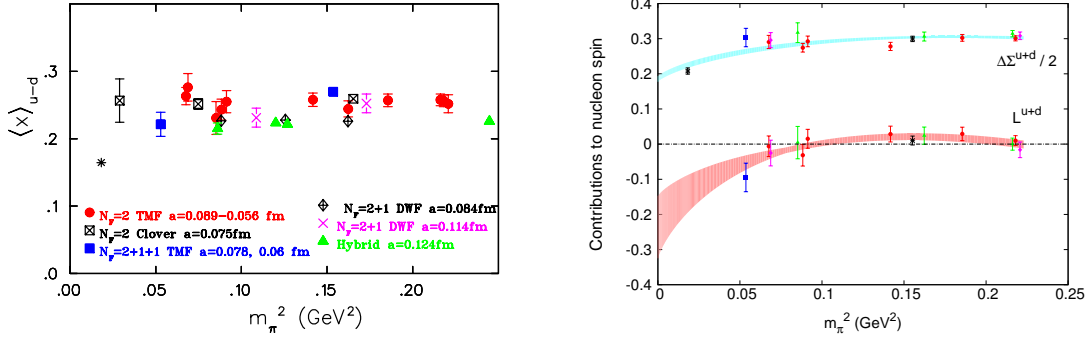


**FIGURE 5.** Left:  $\langle x \rangle_{u-d}$  using  $N_f = 2$  [38] and  $N_f = 2 + 1 + 1$  [32] TMF,  $N_f = 2$  clover fermions [25, 39], hybrid [28] and DWF [40]. The physical point shown by the asterisk is from Ref. [41]. Right: Quark contribution to the nucleon spin and angular momentum using  $N_f = 2$  and  $N_f = 2 + 1 + 1$  TMF.

Neglecting the disconnected contributions to the nucleon spin, one can extract  $J^q$  and  $\Delta\Sigma^q$  using current lattice QCD data. In Fig. 5 we compare recent LQCD results on the isovector momentum fraction  $A_{20} = \langle x \rangle_{u-d}$  in the  $\overline{\text{MS}}$  scheme at a scale  $\mu = 2$  GeV. There is an overall agreement among lattice QCD results and therefore we use TMF results to study the spin content. In Fig. 5 we show the pion mass dependence of the isoscalar spin  $\Delta\Sigma$  and angular momentum  $L$  carried by the u- and d-quarks and in Fig. 6 we show  $J^u$  and  $J^d$  as well as the angular momentum and spin for the u and d quarks. The expressions for the isovector and isoscalar  $J$  and  $\Delta\Sigma$  used in the chiral extrapolations are

$$J^{u-d} = a_1^{IV} m_\pi^2 + a_0^{IV} \left( 1 - \frac{m_\pi^2}{(4\pi f_\pi)^2} ((2g_A^2 + 1) \log \frac{m_\pi^2}{\mu^2} + 2g_A^2) \right)$$

$$\begin{aligned}
J^{u+d} &= a_2^{IS} + a_1^{IS} m_\pi^2 + a_0^{IS} \left(1 - 3g_A^2 \frac{m_\pi^2}{(4\pi f_\pi)^2} \log \frac{m_\pi^2}{\mu^2}\right) \\
\Delta\Sigma^{u-d} &= \tilde{a}_1^{IV} m_\pi^2 + \tilde{a}_0^{IV} \left(1 - \frac{m_\pi^2}{(4\pi f_\pi)^2} ((2g_A^2 + 1) \log \frac{m_p^2}{\mu^2} + 2g_A^2)\right) \\
\Delta\Sigma^{u+d} &= \tilde{a}_1^{IS} m_\pi^2 + \tilde{a}_0^{IS} \left(1 - 3g_A^2 \frac{m_\pi^2}{(4\pi f_\pi)^2} \log \frac{m_\pi^2}{\mu^2}\right)
\end{aligned} \tag{1}$$

At the physical pion mass we obtain a total spin of  $J^u \sim 1/4$  and  $J^d \sim 0$  for the u- and d-quarks, respectively. These results are in agreement with those by the LHPC [28].

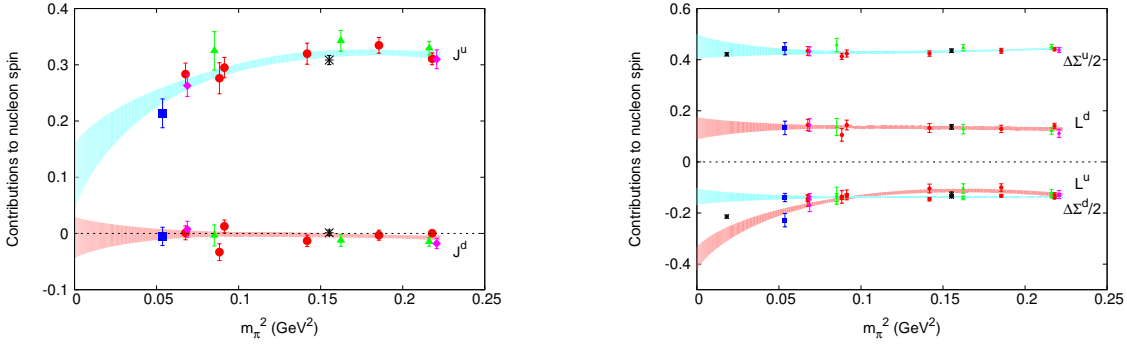


**FIGURE 6.** Spin and angular momentum for u- and d- quarks, for  $N_f = 2$  [38] (filled red, green and magenta symbols) and  $N_f = 2 + 1 + 1$  [32] (filled blue square and black cross) TMF.

## CONCLUSIONS

Recent simulations of lattice QCD successfully reproduce the low-lying baryon spectrum using different discretization schemes paving the way for studying nucleon structure. Key observables such as the nucleon axial charge, rms radii and anomalous magnetic moment, spin and angular momenta carried by quarks are being investigated using simulations with parameters close to their physical values. Understanding well measured quantities, such as  $g_A$ , is crucial in order to reliably predict other less known observables. Simulations currently produced with pion masses below 200 MeV, combined with a detailed study of lattice systematics, are expected to shed light both on the origin of the observed discrepancies and make reliable predictions on other less well known observables.

## ACKNOWLEDGMENTS

I would like to thank my collaborators M. Constantinou, J. Carbonell, S. Dinter, V. Drach, K. Hadjiyiannakou, K. Jansen, C. Kallidonis, T. Korzec, G. Koutsou as well as the other members of ETMC for a very constructive and enjoyable collaboration. This research was partly supported by the Cyprus Research Promotion Foundation project Cy-Tera (NEA

ΥΠΟΔΟΜΗ/ΣΤΡΑΤΗ/0308/31) and ΔΙΑΚΡΑΤΙΚΕΣ/KY-ΓΑ/0310/02 and by the Research Executive Agency of the European Union under Grant Agreement number PITN-GA-2009-238353 (ITN STRONGnet). Results have been achieved using the PRACE Research Infrastructure resource Jugene, and Juropa at JSC, Germany.

## REFERENCES

1. C. Alexandrou, *PoS LATTICE2010*, 001 (2010), 1011.3660.
2. C. Alexandrou, *Prog.Part.Nucl.Phys.* **67**, 101–116 (2012), 1111.5960.
3. C. Alexandrou, C. Papanicolas, and M. Vanderhaeghen (2012), 1201.4511.
4. K. G. Wilson, *Phys.Rev.* **D10**, 2445–2459 (1974).
5. S. Durr, et al., *Science* **322**, 1224–1227 (2008).
6. C. Alexandrou, et al., *Phys. Rev.* **D80**, 114503 (2009), 0910.2419.
7. W. Bietenholz, et al., *Phys.Rev.* **D84**, 054509 (2011), 1102.5300.
8. S. Aoki, et al., *Phys.Rev.* **D81**, 074503 (2010), 0911.2561.
9. A. Bazavov, et al., *Rev.Mod.Phys.* **82**, 1349–1417 (2010), 0903.3598.
10. T. Blum, *PoS LATTICE2008*, 096 (2008).
11. A. Walker-Loud, et al., *Phys.Rev. D* **79** (2009), 0806.4549.
12. Z. Fodor, and C. Hoelbling, *Rev.Mod.Phys.* **84**, 449 (2012), 1203.4789.
13. R. G. Edwards, et al., *Phys.Rev.* **D84**, 074508 (2011), 1104.5152.
14. M. Mattson, et al., *Phys.Rev.Lett.* **89**, 112001 (2002), hep-ex/0208014.
15. J. Russ (2002), hep-ex/0209075.
16. A. Ocherashvili, et al., *Phys.Lett.* **B628**, 18–24 (2005), hep-ex/0406033.
17. B. Aubert, et al., *Phys.Rev.* **D74**, 011103 (2006), hep-ex/0605075.
18. S. Ratti, *Nucl.Phys.Proc.Suppl.* **115**, 33–36 (2003).
19. R. Chistov, et al., *Phys.Rev.Lett.* **97**, 162001 (2006), hep-ex/0606051.
20. H. Na, and S. Gottlieb, *PoS LATTICE2008*, 119 (2008), 0812.1235.
21. L. Liu, H.-W. Lin, K. Orginos, and A. Walker-Loud, *Phys.Rev.* **D81**, 094505 (2010), 0909.3294.
22. R. A. Briceno, D. Bolton, and H.-W. Lin (2011), 1111.1028.
23. C. Alexandrou, J. Carbonell, D. Christaras, V. Drach, M. Gravina, et al. (2012), 1205.6856.
24. J. Green, et al., *PoS LATTICE2012* (2012).
25. D. Pleiter, et al., *PoS LATTICE2010*, 153 (2010), 1101.2326.
26. C. Alexandrou, et al., *Phys.Rev.* **D83**, 045010 (2011), 1012.0857.
27. T. Yamazaki, et al., *Phys. Rev.* **D79**, 114505 (2009), 0904.2039.
28. J. D. Bratt, et al., *Phys. Rev.* **D82**, 094502 (2010), 1001.3620.
29. S. Dinter, et al., *Phys.Lett.* **B704**, 89–93 (2011), 1108.1076.
30. H.-W. Lin, and K. Orginos, *Phys.Rev.* **D79**, 034507 (2009), 0712.1214.
31. C. Alexandrou, et al., *Phys.Rev.* **D83**, 094502 (2011), 1102.2208.
32. C. Alexandrou, et al. (2012), in preparation.
33. S. Collins, et al., *Phys.Rev.* **D84**, 074507 (2011), 1106.3580.
34. S. N. Syritsyn, et al., *Phys. Rev.* **D81**, 034507 (2010), 0907.4194.
35. G. S. Bali, et al., *Phys.Rev.Lett.* **108**, 222001 (2012), 1112.3354.
36. M. Alekseev, et al., *Phys.Lett.* **B693**, 227–235 (2010), 1007.4061.
37. A. Airapetian, et al., *Phys.Rev.* **D75**, 012007 (2007), hep-ex/0609039.
38. C. Alexandrou, et al., *Phys.Rev.* **D83**, 114513 (2011), 1104.1600.
39. A. Sternbeck, et al., *PoS LATTICE2011*, 177 (2011), 1203.6579.
40. Y. Aoki, T. Blum, H.-W. Lin, S. Ohta, S. Sasaki, et al., *Phys.Rev.* **D82**, 014501 (2010), 1003.3387.
41. S. Alekhin, J. Blumlein, S. Klein, and S. Moch, *Phys.Rev.* **D81**, 014032 (2010), 0908.2766.